Molecular architecture of inner dynein arms in situ in *Chlamydomonas reinhardtii* flagella

Khanh Huy Bui,[1] Hitoshi Sakakibara,[2] Tandis Movassagh,[1] Kazuhiro Oiwa,[2,3] and Takashi Ishikawa[1]

[1]Department of Biology, Eidgenössische Technische Hochschule Zürich, CH8093 Zurich, Switzerland
[2]Kobe Advanced ICT Research Center, National Institute of Information and Communications Technology, Iwaoka, Kobe 6512492, Japan
[3]Graduate School of Life Science, University of Hyogo, Harima Science Park City, Hyogo 6781297, Japan

The inner dynein arm regulates axonemal bending motion in eukaryotes. We used cryo-electron tomography to reconstruct the three-dimensional structure of inner dynein arms from *Chlamydomonas reinhardtii*. All the eight different heavy chains were identified in one 96-nm periodic repeat, as expected from previous biochemical studies. Based on mutants, we identified the positions of the AAA rings and the N-terminal tails of all the eight heavy chains. The dynein f dimer is located close to the surface of the A-microtubule, whereas the other six heavy chain rings are roughly colinear at a larger distance to form three dyads. Each dyad consists of two heavy chains and has a corresponding radial spoke or a similar feature. In each of the six heavy chains (dynein a, b, c, d, e, and g), the N-terminal tail extends from the distal side of the ring. To interact with the B-microtubule through stalks, the inner-arm dyneins must have either different handedness or, more probably, the opposite orientation of the AAA rings compared with the outer-arm dyneins.

Introduction

Flagella and motile cilia have highly ordered and precisely assembled superstructures, called axonemes. The most widespread form of the axoneme has a 9 + 2 arrangement of microtubules: nine doublets surrounding a pair of singlets (the central pair microtubules), with radial spokes extending from each of the peripheral doublets toward the central pair.

Coordinated beating and bend propagation of cilia and flagella are generated by active sliding of peripheral doublet microtubules driven by ensembles of various types of dyneins. In the *Chlamydomonas reinhardtii* flagellar axoneme, at least 11 dynein heavy chains (three outer arm and eight inner arm) exist, and each could play crucial and distinct roles in proper flagellar functions (Kagami and Kamiya, 1992). Inner-arm dyneins, which are more essential in flagellar movement than outer-arm dyneins (Kamiya, 1988), are composed of one heterodimeric (dynein f) and six monomeric (dyneins a, b, c, d, e, and g) dyneins, each of which has distinct mechanical properties. Each dynein heavy chain consists of a ring-shaped head and a coiled-coil stalk, as well as an N-terminal tail (referred as a stem in many papers), which folds back and protrudes from the ring next to the stalk (Burgess et al., 2003). Axonemal dyneins show large-scale, integrated behavior that is responsible for the beating of flagella and for wave propagation.

The axonemal dyneins are organized so that a few heavy chains form heterodimers, heterotrimers, or monomers. Studies on an isolated outer-arm dynein show that its heavy chains are tied at the ends of their tails, whereas their globular heads spread apart to form a "bouquet" structure (Johnson and Wall, 1983; Goodenough and Heuser, 1984). In contrast, recent three-dimensional reconstructions of outer dynein arms in situ have demonstrated that their head rings are intimately associated with one another on the microtubule. Electron tomography of metal replicas of rapidly frozen and cryo-fractured sperm axonemes from the dipteran *Monarthropalpus flavus* (Lupetti et al., 2005), cryo-electron tomography of sea urchin sperm (Nicastro et al., 2005) and *C. reinhardtii* flagella (Nicastro et al., 2005, 2006; Ishikawa et al., 2007), and in vitro cryo-electron microscopy studies of reconstituted outer-arm dyneins (Oda et al., 2007) have shown that an outer dynein arm is composed of two or three stacked plates, which correspond to the head rings. However, the architecture of the inner dynein arm has not been described.

Correspondence to Takashi Ishikawa: takashi.ishikawa@mol.biol.ethz.ch

Abbreviations used in this paper: DRC, dynein regulatory complex; IC, intermediate chain; LC, light chain.

The online version of this article contains supplemental material.

The Rockefeller University Press $30.00
J. Cell Biol. Vol. 183 No. 5 923–932
www.jcb.org/cgi/doi/10.1083/jcb.200808050

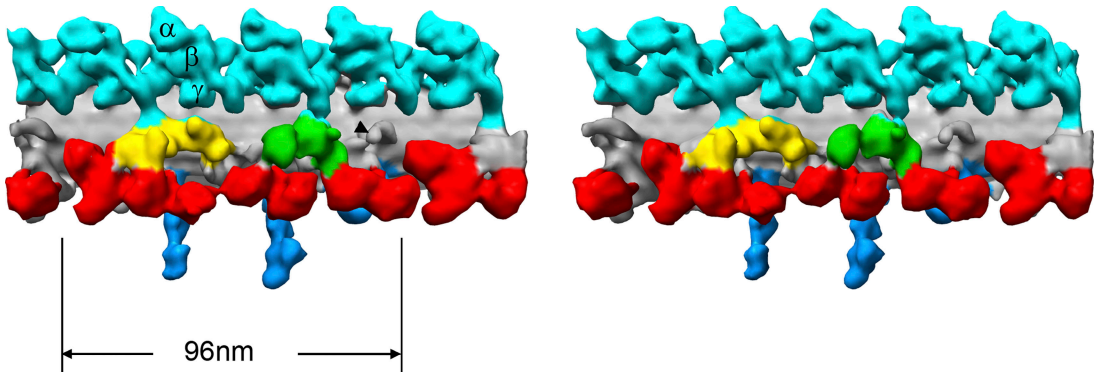

Figure 1. **Surface rendering (stereo view) representation of the three-dimensional structure of the *C. reinhardtii* flagellum.** The representation includes the A-microtubule, outer dynein arms (light blue), inner dynein arms (red), the IC–LC of the inner dynein arms (yellow), the DRC (green), and radial spokes (RS; blue) colored based on Porter (1996) within a 96-nm repeat. AAA rings of the three heavy chains in one outer dynein arm are also indicated. The black arrowhead indicates the candidate of nexin.

According to the electron microscopy of freeze-fracture, deep-etched cilia by Goodenough and Heuser (1985), a triad and two dyads of dynein heavy chains are formed around the three radial spokes (S1, S2, and S3, respectively) in *Tetrahymena thermophila*. Piperno et al. (1990) found that, based on plastic-embedded sections of *C. reinhardtii* flagella, there are three domains (referred as I1, I2, and I3) in every 96-nm repeat of the inner dynein arms. Burgess et al. (1991) compared both the freeze-fracture, deep-etched replica and the section of sperm flagella from *Gallus domesticus* and concluded that inner dynein arm 1 (IDA1) consists of four dynein heavy chains, whereas IDA2 and IDA3 consist of two dynein heavy chains each. By comparing electron micrographs of plastic-embedded flagella from *C. reinhardtii*, the positions of a few isoforms of dynein heavy chains on the A-microtubule were mapped (Mastronarde et al., 1992; Yagi et al., 2005). Nicastro et al. (2006) clarified the position of dynein f (dynein I1) by comparing the structure of the wild type and *pf9* mutant. Nevertheless, precisely how dynein heavy chains of inner dynein arms are organized into the complexes in the axoneme remains unknown. In particular, to understand the mechanism of flagellar motion, the conformation of the rings and the tails of the eight inner-arm dynein heavy chains requires detailed description in three dimensions.

In our study, we use *C. reinhardtii* flagella because many useful mutants of dyneins and several axonemal components have been isolated and characterized, making *C. reinhardtii* a useful model for structural studies of the axoneme. We use the techniques of cryo-electron tomography and single particle averaging, and describe the three-dimensional molecular configurations of inner dynein arms and positions of the N-terminal tails of all the eight heavy chains of inner dynein arms. We provide evidence that six heavy chains (dynein a, b, c, d, e, and g) are roughly colinear, with N-terminal tails emerging at the distal side of the rings. Six monomeric heavy chains form three dyads (although these dyads do not necessarily correspond to the dyads described previously; Goodenough and Heuser, 1985) around two radial spokes, and one structure similar to the radial spoke.

The results suggest that monomeric inner-arm dyneins work as functional dimers in the axoneme. Together with functional analyses of dynein mutants, the results support the idea that not all dyneins are necessary, but the presence of certain combinations of dyneins seems to be crucial for the correct functioning of the axoneme (Kamiya, 2002).

Results

Electron cryo-tomography and three-dimensional single particle averaging using the periodic structure (96-nm repeat) were used to reconstruct the three-dimensional structure of the flagellar inner dynein arm from *C. reinhardtii* in the absence of nucleotides, together with the microtubule doublet (A-microtubule), outer dynein arms, and part of the radial spokes (Fig. 1). We can easily distinguish the outer dynein arms and microtubule doublets we have already described (Ishikawa et al., 2007) from inner dynein arms, as indicated in color in Fig. 1. To identify the components of the inner dynein arm, we reconstructed the structures of the following mutants (Table I): *oda1*, *ida1*, *ida5*, *ida2-6::λC(D11)*, *ida9*, *ida4*, *pf2*, *pf3*, and *sup-pf3* (Fig. 2).

Overall arrangement of the inner dynein arm

In the three-dimensional map (Fig. 1), several bulbs are clearly seen in the inner dynein arm (they are shown from a different view angle in Fig. 3). Six of them are located as one straight array along the length of the A-microtubule at ∼180 Å from the surface (Fig. 4, A and B, red arrows; Fig. 4 E shows the surface of the A-microtubule). The AAA rings of the heavy chains are almost parallel to the surface of the A-microtubule, as seen in Fig. 4 (B and E), with slight variations (described in detail in the next section). Judging from the distances between adjacent AAA rings, the six rings associate pairwise to form three dyads, which we call dyads 1, 2, and 3, seen from the proximal side (Fig. 3 A). Radial spokes (S1 and S2) adjoin dyads 1 and 2 (Fig. 3, arrowheads), respectively. Because there are only two radial spokes in *C. reinhardtii*, there is no counterpart for the third dyad, but there is a protrusion (Fig. 3 A, arrows) that is based on the same protofilament of the A-microtubule, extending toward the center of the axoneme,

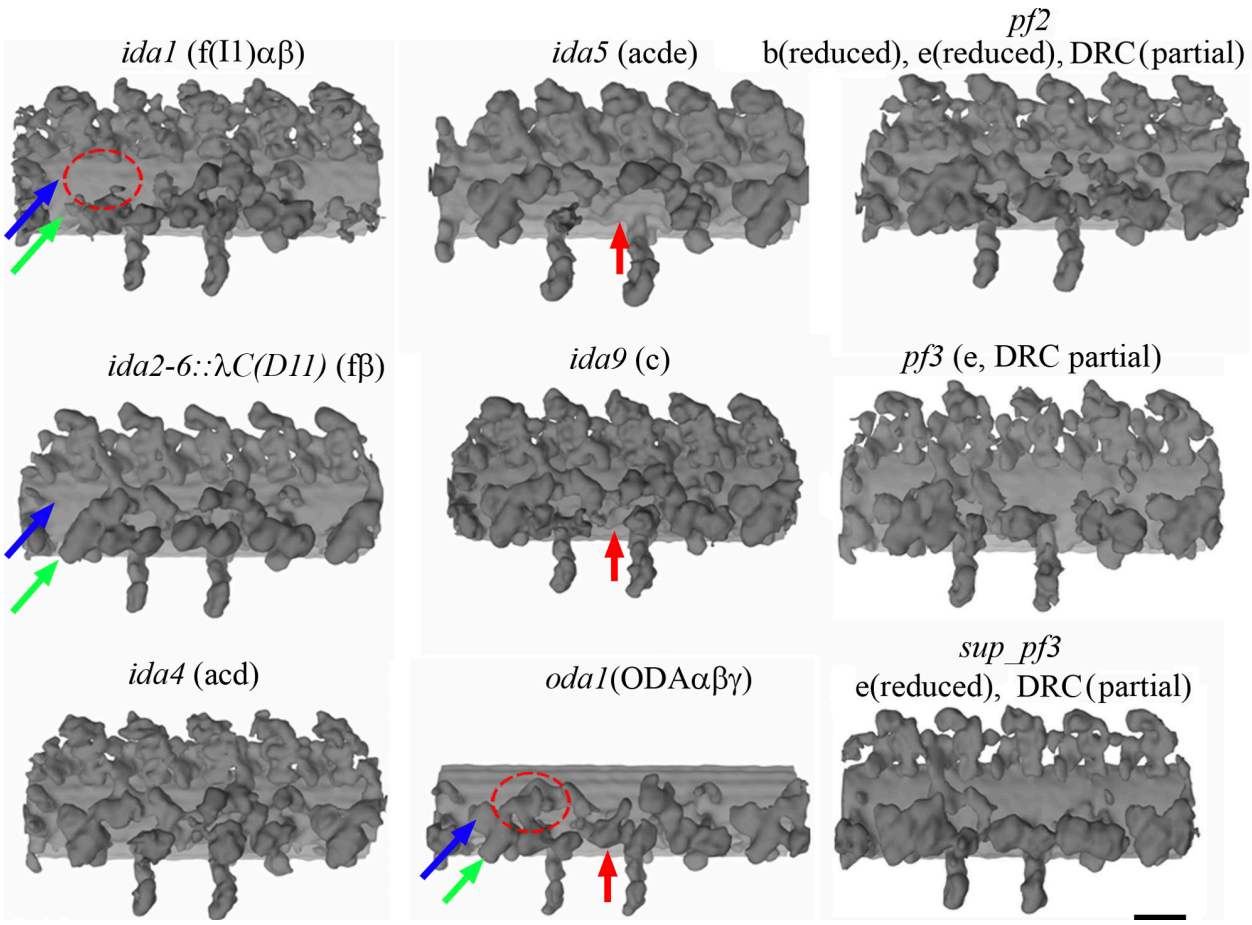

Figure 2. **Three-dimensional structure of mutants.** Components missing in each mutant are indicated in parenthesis. In *ida1*, *ida2-6::λC(D11)*, *ida5*, *ida9*, and *oda1* mutants, the locations of a dynein f dimer (blue and green) and dynein c (red) are indicated by arrows, whereas the location of the LC–IC complex of dynein f is encircled by red dotted circles. Bar, 20 nm.

and that has a similar diameter to the base of the radial spokes (Fig. 3 A). This protrusion is located 240 Å distal from spoke II and docks on the same protofilament as spokes I and II. This position is identical to that of the third radial spoke in *T. thermophila* (unpublished data; Avolio et al., 1986; Taylor et al., 1999). The other two bulbs are closer to the surface of the A-microtubule, one at ∼60 Å and closer to the outer dynein arms, whereas the other is ∼130 Å away from the A-microtubule (Fig. 4, C and D). All these features of the inner dynein arm are common between the wild type and the *oda1* mutant, which lacks the outer dynein arm (Fig. 3 B), demonstrating that the architecture of the inner dynein arm and the radial spoke is maintained independently of the outer dynein arm. According to the structural study of the reconstituted outer dynein arm (Oda et al., 2007), the three AAA rings of the outer dynein arm can stack together as in intact flagella,

Table I. Characteristics of mutants used in this study

Strain	Missing components	References	Number of particles averaged in this work
Wild type			559
oda1	Outer dynein arms	Kamiya, 1988	656
ida1	f	Piperno et al., 1990; Kamiya et al., 1991; Kagami and Kamiya, 1992; Kremer et al., 1996;	471
*ida2-6::λ*C(D11)	f (1β)	Perrone et al., 2000	897
ida4	a, c, and d	Kamiya et al., 1991; Kagami and Kamiya, 1992	877
ida5	a, c, d, and e	Kato et al., 1993	754
ida9	c	Yagi et al., 2005	955
pf2	b (reduced), e (reduced), and DRC (partial)	Gardner et al., 1994; Rupp and Porter, 2003	530
pf3	e and DRC (partial)	Gardner et al., 1994; Piperno et al., 1994	391
sup-pf3	e (reduced) and DRC (partial)	Gardner et al., 1994; Porter et al., 1992	365

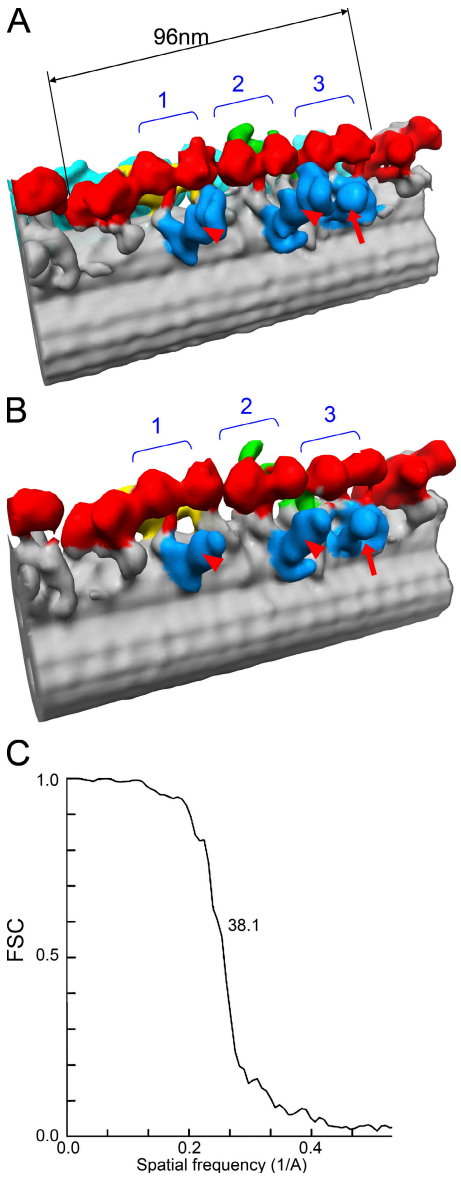

Figure 3. **Three-dimensional reconstruction of flagella from the wild type and a mutant.** Surface rendering representations of the wild type (A) and *oda1* (B) flagellum seen from a different angle compared with Fig.1. Six of eight dynein heavy chains form three dyads in the inner dynein arm. (left) The proximal end. (right) The distal end. Two radial spokes (red arrowheads) and one protrusion (red arrows) are associated with the three dyads, respectively. Stereo pairs are shown in Fig. S1 (available at http://www.jcb.org/cgi/content/full/jcb.200808050/DC1). Online supplemental videos are also available. (C) Fourier shell correlation curve of the *oda1* mutant.

although the N-terminal tails were not visualized, probably because they are not fixed without the support of inner dynein arms. Because we obtained the structural information at the highest resolution so far with *oda1* (~38 Å; Fig. 3 C; the resolution of the wild type is 41 Å [not depicted]) and it is easy to observe the inner dynein arm in the *oda1* mutant without being blocked by outer dynein arms, we discuss the architecture of the inner dynein arm based on *oda1*. Stereo views of the wild type and *oda1* are shown in Fig. S1 (available at http://www.jcb.org/cgi/content/full/jcb.200808050/DC1).

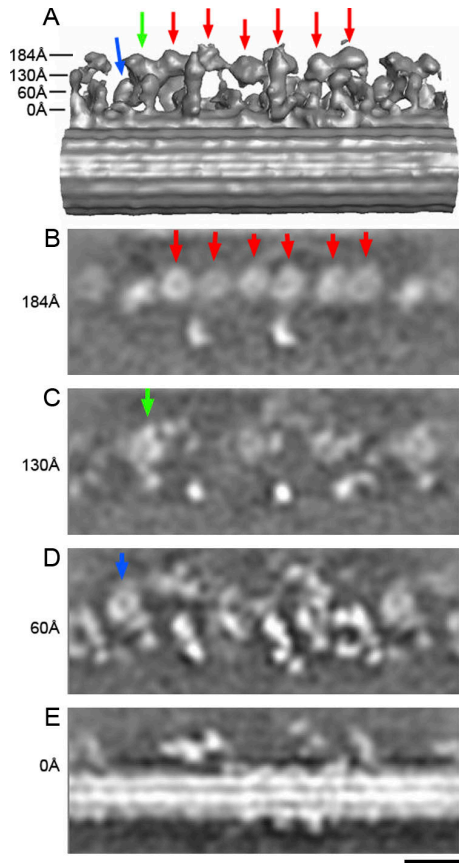

Figure 4. **Horizontal sections from the three-dimensional density map of the *oda1* mutant at various heights.** Arrows in A indicate the heights in the surface rendering model. The six AAA rings (to be assigned as dynein a, b, c, d, e, and g later), and dynein fα and fβ are shown by red, green, and blue arrows, respectively. In horizontal sections (B, C, and D), six of the eight DHC rings are at the same height, whereas two are located closer to the A-microtubule. Bar, 20 nm.

Localization and orientation of the eight AAA rings

In the horizontal sections of the *oda1* mutant (i.e., parallel to the microtubule), all the eight bulbs mentioned in the previous paragraph were proved to be rings (Fig. 4, arrows), as we have already seen in the outer dynein arm (Ishikawa et al., 2007), which indicates that they are AAA rings of eight dynein heavy chains. Six of them are located at almost the same height (Fig. 4, red arrows), whereas another (Fig. 4, green arrow) is closer to the A-microtubule, and the other (blue arrow) is the closest. By extracting the density map corresponding to the rings, projecting from various view angles to find the projection most similar to a circle (Figs. 5 A and S2, available at http://www.jcb.org/cgi/content/full/jcb.200808050/DC1), we detected the orientations of these rings (Fig. 5 B). The ring 130 Å away from the A-microtubule (later found to be dynein fα) and the proximal ring in the third dyad (later found to be dynein b or g) are tilted significantly (~35° about an axis transverse to the microtubule). However, the other six rings are almost parallel to the surface of the A-microtubule. The angles of the eight AAA rings from *oda1* are common among the wild type and mutants reconstructed in this study (not depicted).

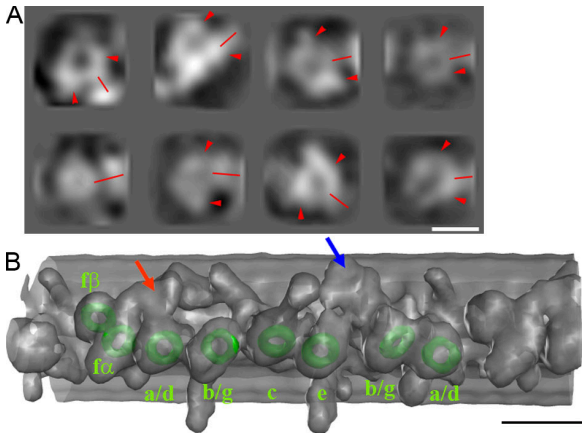

Figure 5. **Detection of the AAA rings in the density map of the *oda1* mutant.** (A) The eight rings detected in the 96-nm repeat of the *oda1* mutant as projections. (left) Proximal end. (right) Distal end. N-terminal tails, which project out between two bulky densities (arrowheads), are shown by red lines. (B) Orientations of the eight rings are shown. Isoforms of dynein heavy chains are indicated by green rings based on Fig.2. LC–IC complex and DRC are shown by red and blue arrows, respectively. A stereo view of B is shown in Fig. S1 (available at http://www.jcb.org/cgi/content/full/jcb.200808050/DC1). Bars: (A) 10 nm; (B) 20 nm.

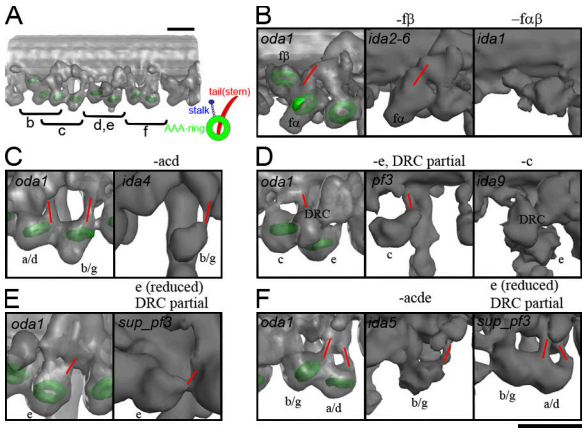

Figure 6. **Detailed comparisons between *oda1* and other mutants reveal the location of the AAA rings and the N-terminal tails of the eight dynein heavy chains.** In each panel, the orientation is slightly different in order to show the rings and the tails, but the distal end is always at the right (the proximal side is at the left). Approximate positions and the model of one dynein heavy chain (right bottom; green, AAA ring; red, N-terminal tail [stem]; blue, coiled-coil stalk and microtubule-binding domain) are shown in A. The rings and the tails are shown by green rings and red lines, respectively. Two tails of the dynein f dimer merge (B), whereas pairs of heavy chains belonging to one dyad have a colinear architecture, with the N-terminal tails projecting from the distal sides of the rings without merging (C–F). Bar, 20 nm.

Identification of the eight AAA rings, light chain–intermediate chain (LC–IC) complexes, and dynein regulatory complex (DRC) by comparison of mutants

By comparing the *oda1* mutant (or the wild type) with various mutants (Fig. 2), we identified eight dynein heavy chains. The ring closest to the A-microtubule and the outer dynein arm seen in *oda1* disappeared in *ida2-6::λC(D11)*, which lacks dynein fβ (Fig. 2, blue arrows). The other component of dynein f (dynein fα; Fig. 2, green arrows) was identified by comparison with *ida1*, which lacks both heavy chains of dynein f. Dynein c, which *ida9* lacks, can be localized at the second dyad (with the S2 radial spoke; Fig. 2, red arrows). In *ida4* (lacking dyneins a, c, and d) and *ida5* (lacking a, c, d, and e), this ring cannot be seen, which supports this assignment. Another ring belonging to the second dyad should be assigned as dynein e because it does not exist in the *pf3* mutant (lacking dynein e). This ring also disappears in *pf2*, in which the amount of dynein e is decreased (Gardner et al., 1994).

There is no *C. reinhardtii* mutant to distinguish dynein a and d or dynein b and g. Hence, as seen in *ida5* (lacking a, c, d, and e) and *ida4* (lacking a, c, and d), we should assign the proximal ring of the first dyad and the distal ring of the third dyad as dynein a or d. Consequently, the distal ring of the first dyad and the proximal ring of the third should be dynein b and g. The assignment of all the eight heavy chains is shown in Fig. 5 B (stereo pairs are shown in Fig. S1). There are two other bulbs in the map. One (Fig. 5 B, red arrow) disappears in *ida1* (lacking dynein f; Fig. 2, encircled with a red dotted line) and must correspond to the LC–IC complex of dynein f. The density of the other bulb (Fig. 5 B, blue arrow) decreases significantly in *pf2*, *pf3*, and *sup-pf3* mutants, indicating that this bulb is the DRC. The structures of the IC–LC complex and the DRC (Fig. 1, yellow and green) are consistent with previous work (Nicastro et al., 2006).

Dynein f

Two AAA rings of dynein f are located closer to the surface of the A-microtubule than the rest of AAA rings. Dynein fβ is quite near (~80 Å) the surface of the A-microtubule, whereas dynein fα is at a longer distance (~130 Å; Fig. 4, C and D). The two rings of the dynein f dimer and the LC–IC complex are connected by one single rod (Fig. 6 B, red line). The views seen from the opposite orientation are shown in Fig. S3 (available at http://www.jcb.org/cgi/content/full/jcb.200808050/DC1). This rod remains in the *ida2-6::λC(D11)* mutant, which lacks the fβ heavy chain, but disappears when both heavy chains are missing in *ida1*. Although there is another continuous strand of density between the fβ ring and the adjacent ring (later found to be dynein a or d), this density remains in *ida1* and, thus, cannot be assigned as the tail of fα. The only possible assignment here is the double-headed dimer with one common rod, like myosin and kinesin. This is consistent with negative staining electron microscopy of purified dynein f (Kotani et al., 2007), which showed two head domains relatively closely apposed at one end of an elongated structure. When these ring-shaped structures are projected (Fig. 5 A, first two panels), two prominent density bulbs are observed in one ring (Fig. 5 A, arrowheads) as well as a tail protruding from the gap between the two bulbs (red lines), which is consistent with the two-dimensional averaging of the negatively stained dynein c (Burgess et al., 2003).

Arrangement of the rings and tails of dynein a–e and g

We compared the detail of the *oda1* mutant, which retains all the components of the inner dynein arm, and other mutants that lack inner dynein arm components, to localize these components. The N-terminal tails of the six heavy chains can be localized in this way. In *ida4* (lacking a, c, and d), a rod seen in *oda1*

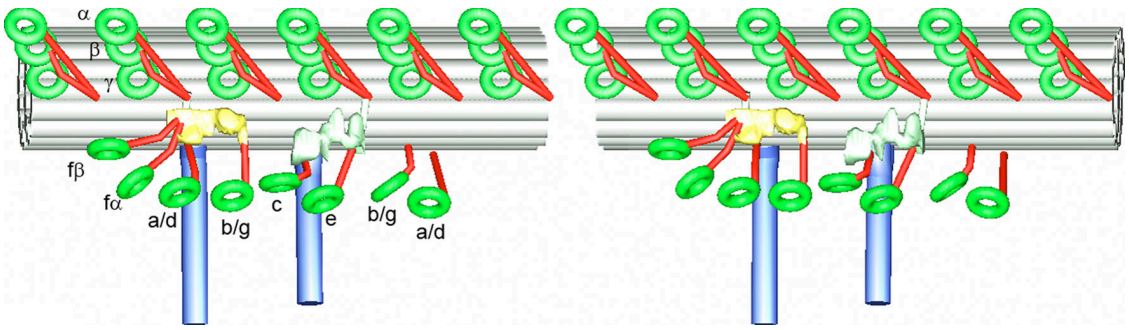

Figure 7. **Schematic diagram of the arrangement of the inner and outer dynein arms (stereo view).** The rings belonging to the inner and outer dynein arms are shown as green rings. The N-terminal tails are shown in red.

(Fig. 6 C, red lines) bridging between the A-microtubule and dynein a or d disappears, whereas another rod connecting b/d and the A-microtubule remains in *ida4* (Fig. 6 C), which indicates that the rods are the tail of a/d and b/g, respectively. In the same way, the comparison between *oda1* and *pf3* (lacking e), between *oda1* and *ida9* (lacking c), and between *oda1* and *sup-pf3* (e reduced) clarifies the location of the e-tail and the c-tail (Fig. 6, D and E). Comparison of *oda1*, *sup-pf3*, and *ida5* (lacking a, c, d, and e; Fig. 6 F) enables the assignment of the tails of b/g and a/d in the third dyad. In summary, in all the six dynein heavy chains, the tails emerge at the distal (i.e., the orientation toward the tip of the flagella) side of the AAA rings. Each tail is indicated in projection as well (Fig. 5 A). There, it is shown that all the tails emerge roughly at the distal side of the rings, but with slight variation. The surface rendering presentation also shows the difference of the conformation of the tail. For example, the attachment points of the N-terminal tails of the first dyad appear to point away from each other (Fig. 6 C), whereas the tails of the third dyad point toward each other (Fig. 6 F).

Connection between inner and outer dynein arms

As seen in Fig. 1, there are two connections between the outer and inner dynein arms in the 96-nm repeat, as described previously in Nicastro et al. (2006). One is between DRC and the "internal bulb" assigned as N-terminal tails of α- and β-heavy chains of the outer dynein arm (Ishikawa et al., 2007), whereas the second connection 48 nm away from the first binds to the LC–IC complex of dynein f. The structure of the outer dynein arm is similar to our previous study reconstructed with 24-nm periodicity. The locations of components identified in the 96-nm periodicity are summarized in Fig. 7.

Discussion

Eight heavy chains

According to the genomic study of *C. reinhardtii*, 11 genes are known to code for heavy chains of the inner dynein arm (Perrone et al., 2000). However, only eight dynein heavy chains have been detected biochemically (Kagami and Kamiya, 1992), and the rest of the heavy chains are thought to be rarely expressed or localized in a restricted area (e.g., close to the basal body or at the tip; see Yagi, T., personal communication in King and Kamiya, 2008). Our observation of the eight rings in the 96-nm repeat is consistent with these previous studies. Six of the eight heavy chains seem to form three dyads, judging from the distance between them, although it is not clear how these dyads are relevant to the "triad, dyad, dyad" structure described previously (Goodenough and Heuser, 1985). Because the first, second, and third are close to the radial spokes S1 and S2, and the feature at the location of S3 of *T. thermophila*, respectively, it is likely that the two dyads in the previous work correspond to our second and third dyads, whereas their triad corresponds to our first dyad and dynein f. If this assignment is correct, the position of the protrusion seen in Fig. 1 (arrowhead), is the same as that of nexin described in Bozkurt and Woolley (1993). The density of the distal AAA ring of dyad 1 (to be assigned as b or g; Fig. 4 B, second red arrow from the left) is weaker than the other heavy chain rings, presumably because of flexibility or heterogeneity. In the previous study by electron cryo-tomography (Nicastro et al., 2006), this ring was not visualized. Averaged rings of dynein c and dynein e (Fig. 5 A, the first and the second images in bottom row) appear more ambiguous as rings than the other six rings, and suggest heterogeneity.

We identified these heavy chains in the three-dimensional reconstruction using mutants. Our three-dimensional localization of eight heavy chains is consistent with previous two-dimensional mapping studies based on the electron microscopy of plastic-embedded sections (Mastronarde et al., 1992; Gardner et al., 1994; Porter, 1996; Yagi et al., 2005), although there are a few minor differences. For example, in Fig. 5 I of Yagi et al. (2005), in the first and second dyads, dynein a/d and dynein c were assigned close to the radial spokes S1 and S2, respectively. However, in our reconstruction, each counterpart ring in the dyad, e.g., dynein b/g and dynein e, are close to S1 and S2, respectively. Most likely, the density difference between the mutant and the wild type obtained from plastic-embedded sections reflects the density of the N-terminal tails, which are localized at the distal side compared with the AAA rings.

It is still impossible to distinguish two pairs; a or d and b or g. Because there are no mutants that lack a but not d (or vice versa), or lack b but not g (or vice versa), we need either antibodies to bind them specifically or new mutants. Although many mutants of flagella or dyneins of *C. reinhardtii* make it a valuable experimental system for studies of the structure and function of dyneins, *T. thermophila* may help to complete the mapping of

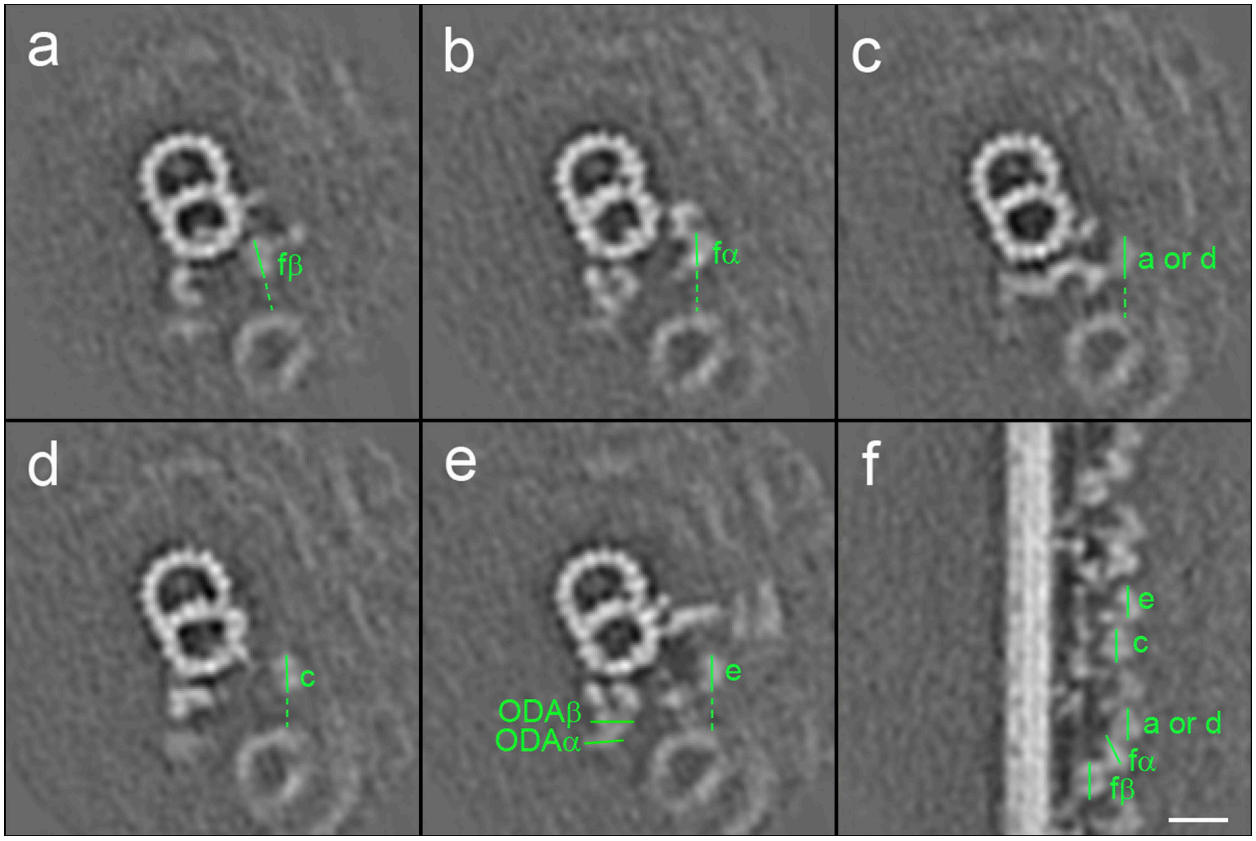

Figure 8. **Sections of the density map of the wild type.** (a–e) Vertical sections (perpendicular to the microtubule) of the wild-type flagellum. AAA rings of the heavy chains of inner and outer dynein arms are marked by green lines. The solid lines show the sections of the planes of the rings. Corresponding locations and the orientations of the inner arm dynein rings are shown in the longitudinal section (f; so the lines in a–e and the lines in f are perpendicular to each other). (a) The section including dynein fβ. (b) Dynein fα. The distance from a is 75 Å. (c) Dynein a or d (180 Å from a). (d) Dynein c (450 Å from a). (e) Dynein e (580 Å). Dotted lines are extensions in the same plane as the rings and are presumed to represent the orientation of the stalks. ODA, outer dynein arm. Bar, 20 nm.

inner-arm dyneins because the established methodology of homologous recombination is applicable to design mutants.

Three dyads of heavy chains and radial spokes

As shown in Fig. 3, six AAA rings of heavy chains (a, b, c, d, e, and g) form three horizontal dyads. The first (a or d, and b or g) and the second (c and e) dyads are close to the radial spokes S1 and S2, respectively, whereas the third (b or g, and a or d) is close to a structure similar to a radial spoke at the same location as the third radial spoke in *T. thermophila* (Goodenough and Heuser, 1985). Previous biochemical studies (Piperno et al., 1992; LeDizet and Piperno, 1995; Yanagisawa and Kamiya, 2001) indicated that dynein a, c, and d have actin and p28 as LCs, whereas dynein b, e, and g have actin and centrin as LCs. Our results showed that each of the three dyads should contain both p28 and centrin simultaneously, which suggests that actin, p28, and centrin are essential and cooperative for regulation. If the dyads work as functional dimers, these LCs may interact with each other through yet unrevealed components.

Interaction with the B-microtubule

In our current study, the stalks are not visible. However, the orientations of the AAA rings provide some information on the interaction between the AAA rings and the B-microtubule. In Fig. 8, the orientations of the plane including the AAA ring of each inner and outer heavy chain are shown by green solid lines, in vertical sections (the location of each section is shown in the longitudinal section; Fig. 8 f, where green lines show perpendicular sections to those in Fig. 8, a–e). When these planes are extended (Fig. 8, green dotted lines), they reach the B-microtubule. This suggests that the α and β rings of the outer dynein arm and the inner dynein arm heavy chains contact the B-microtubule, probably through their stalks. As seen in Fig. 8 f (green lines show the sections of the plane involving the AAA rings), the AAA rings of dynein a or d, c, e, and fβ are parallel to the microtubule. This architecture enables them to drive the B-microtubule linearly. In contrast, the ring of dynein fα is tilted (~35° as mentioned in Results; Fig. 8 f, indicated by a green line and marked "fα"). Although dynein fα is close enough to the B-microtubule (Fig. 8 b), the stalk may swing in a different orientation or can generate torques. In in vitro motility assays, dynein f does not rotate microtubules in a corkscrew-like manner while moving forward. In contrast, dynein a, b, c, and g show corkscrewing of microtubules (Kikushima and Kamiya, 2008). These observations suggest that the power stroke of these dyneins is three dimensional in vitro. However, because the arrangement of fα is different from other dyneins in vivo, the sliding of the microtubule

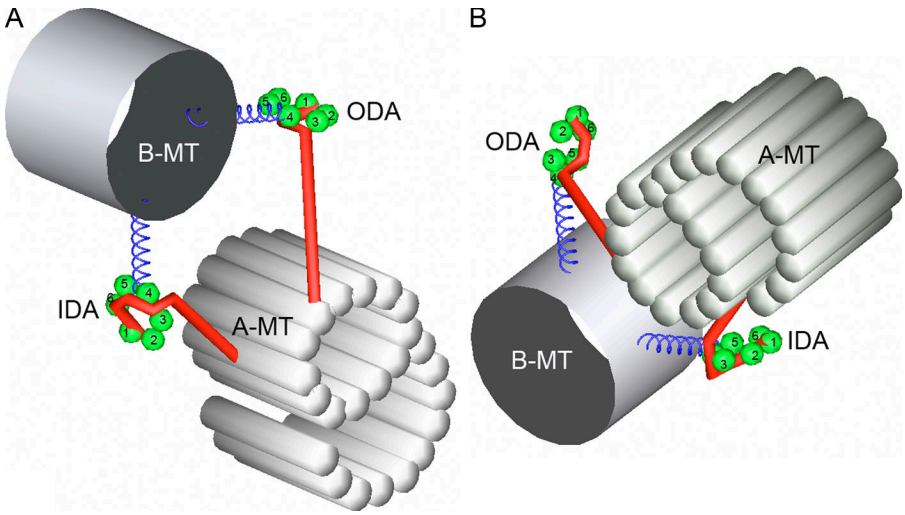

Figure 9. **Schematic diagram of the conformation of heavy chains in the inner and outer dynein arms.** (A) The view from the B-microtubule (B-MT). (left) Proximal side. (right) Distal side. (B) The view from the A-microtubule (A-MT). (left) Distal side. (right) Proximal side. The AAA domains are marked. The assignment and the conformation of the six AAA domains (green balls) in each ring, the coiled-coil stalks (blue helices), and the N-terminal tails (red rods) are based on Burgess et al. (2004). The likely arrangement of the six AAA domains is indicated based on the two-dimensional averaging of dynein c (Burgess, S., personal communication). Combining this indexing and three-dimensional reconstruction of cytoplasmic dynein (Samso and Koonce, 2004), we speculate that the tail wraps around the AAA ring, as shown here. IDA, inner dynein arm; ODA, outer dynein arm.

by fα in vivo could be different from that in vitro. In our previous study, we proposed the possibility that the γ heavy chain has a different orientation and thus could have a different function from the other two heavy chains (Ishikawa et al., 2007). This would be the case for dynein fα. Furthermore, the study on dynein f mutants, which have truncated heavy chains, shows that α and β heavy chains have distinct activities in ATPase and motility (Toba, S., C. Mellor, N. Kotani, H. Sakakibara, H. Kojima, J. Molloy, and K. Oiwa. 2008. Proceedings of the Biophysical Society. Abstr. 1824). Here, the distinct arrangement in vivo and functions in vitro of dynein fα may suggest a function of dynein fα different from other heavy chains and may explain the regulation mechanism of dynein f through phosphorylation of its IC (Hendrickson et al., 2004; Dymek and Smith, 2007; Wirschell et al., 2007).

Conformation of heavy chains in the inner dynein arm in situ

Both the heavy chains (α and β) from the outer dynein arm and all the heavy chains from the inner dynein arm have tails emerging at the distal side of the rings and extending toward the distal end of the axoneme (Fig. 7). In both inner- and outer-arm dyneins, the rings are nearly parallel to the surface of the A-microtubule (Fig. 5 b). When the plane involving a ring is extended, it can reach the adjacent B-microtubule (Fig. 8), which suggests that the stalk, which is not visible in the present study, is in the same plane as the ring and interacts with the B-microtubule. In contrast, the tail is bent (or tilted) to reach the surface of the A-microtubule, and, consequently, it cannot be in the same plane as the AAA ring (shown in Fig. 9). This is the basic conformation of the heavy chains, at least the α and β heavy chains of the outer dynein arm and dynein a, b, c, d, e, and g of the inner dynein arm (Fig. 9). According to the previous study on dynein c by Burgess et al. (2003), the C terminus of the N-terminal tail (mentioned as a stem), called the linker, folds back on the AAA ring. In the outer dynein arm (at least the α and β heavy chains), in order to be able to extend toward the adjacent B-microtubule for the sliding motion, the stalk must emerge at the right side when viewed from the proximal side (Fig. 9). However, in the case of the inner dynein arm, the stalk must emerge from the left side of the ring (viewed from the proximal side to the distal side) to reach the adjacent B-microtubule (Fig. 9). This means that the stalks from the inner dynein arm and outer dynein arm project from opposite sides for the inner and outer dynein arms (Figs. 7 and 9). One possible explanation is that the rings of the outer and inner dynein arms present opposite faces to the A-microtubule (Fig. 9). The tails of both outer and inner dynein arms extend out of the plane of the AAA rings, but in opposite directions (Fig. 9). With these architectures, both the outer and inner dynein arms can drive the B-microtubule in the same (plus-end) orientation. We further speculated the positions of the six AAA domains based on the recent structural study on cytoplasmic dynein by S. Burgess (personal communication; indexed in Fig. 9). If the three-dimensional conformation of cytoplasmic dynein (Samso and Koonce, 2004) is the same as that of axonemal dynein, the linker region of the N-terminal tail should wrap around the AAA ring, as shown in Fig. 9. Another possibility is that inner- and outer-arm dyneins have a distinct handedness, though this is less likely.

The architecture of the heavy chains discussed in this paper, which is indispensable to reveal the mechanism of the function of each isoform, will have to be experimentally clarified by visualizing the coiled-coil stalks, which are responsible for ATP-sensitive binding to B-microtubules. This will require a technical breakthrough or a combination with other methodologies, e.g., rotary shadowing (Lupetti et al., 2005).

Materials and methods

Cell culture and flagella purification

C. reinhardtii 137c (wild-type; mating type +) and additional mutants described in Table I were cultured using tris-acetate-phosphate (TAP) medium (Gorman and Levine, 1965). For some mutants, culturing in TAP minimum medium without acetate (Gorman and Levine, 1965) for 1 h to induce flagellar growth before deflagellation was needed. Flagella were isolated using dibucaine to induce deflagellation as described previously (Witman, 1986). The separated, intact axonemes were centrifuged at 5,200 *g* for 60 min at 4°C. The pellet was resuspended in 30 mM Hepes, pH 7.4, 5 mM $MgSO_4$, 1 mM DTT, 0.5 mM EDTA, 25 mM KCl, and 0.5% (wt/vol) polyethylene glycol (MW 20,000) and stored at 0°C. No nucleotides were added during isolation of the flagella.

Quick freezing and electron cryo-tomography

The specimen was frozen with liquid ethane at liquid nitrogen temperature using the Vitrobot (FEI Company) and transferred to a cryo-holder (626;

Gatan) at liquid nitrogen temperature. Images were collected as described previously (Ishikawa et al., 2007) using a transmission electron microscope (Tecnai F20; FEI) equipped with a field emission gun, a GIF Tridiem energy filter (Gatan) and a 2,048 × 2,048 charge-coupled device camera (Gatan) at the accelerating voltages of 200 kV, a magnification of 19,303×, and an underfocus of ∼2–4 µm. Tomographic image acquisition from −60° to 60° (2° increment angle) was performed with Explore3D (FEI company).

Image reconstruction

For data from the wild type and all mutants, the same image analysis procedures were applied. The acquired image datasets were aligned using gold beads as fiducial markers and then reconstructed by R-weighted back projection using IMOD (Kremer et al., 1996; Mastronarde, 1997). Subtomograms with dimension of 200 × 200 × 200 pixels (∼144 nm in each dimension, hence covering more than one 96-nm repeat of inner dynein arms) along each microtubule were extracted three-dimensionally by Bsoft (Heymann, 2001). Subtomograms along the same doublet were first aligned using the average of those subtomograms without alignment as the reference and then averaged. Then, the obtained subaverages for each doublet were aligned with a chosen subaverage as the reference using SPIDER (Frank et al., 1996) and the TOM software toolbox (Nickell et al., 2005). The number of particles used for averaging of each mutant is shown in Table I. The averaged map was then deconvoluted by dividing its Fourier transform by the weight from the contributions of all particles' missing wedges. Surface rendering was done by Chimera (Pettersen et al., 2004) after masking, and denoising was performed with a bandpass filter and contrast inversion. For some noisy averages, the "unblob" Chimera Python script (provided by T.D. Goddard, University of California, San Francisco, San Francisco) was used to remove small unconnected fragments of density. The orientation of the rings were evaluated by extracting 30 × 30 × 30 voxels (corresponding to ∼210 Å), projected from various euler angles (θ and φ ranging from 0 to 90° and from 0 to 180°, respectively, with a 5° increment angle). The three-dimensional model of the wild type and the model of A- and B-microtubule interaction through outer and inner dynein arms were built from tracing the electron density map using IMOD (Kremer et al., 1996).

Online supplemental material

Fig. S1 contains the stereo view of Fig. 3 (A and B) and Fig. 5 B. Fig. S2 shows the montages of several two-dimensional projections of various angles of the AAA ring of dynein fβ extracted three-dimensionally from the average tomogram in order to search for the ring orientation. Fig. S3 shows the detailed comparisons between *oda1* and other mutants from a different view from Fig. 6 for assignment of the tails. Videos 1 and 2 show the surface rendering of the average volume of wild-type *C. reinhardtii* and *oda1* mutant, respectively. Online supplemental material is available at http://www.jcb.org/cgi/content/full/jcb.200808050/DC1.

We thank Prof. T. J. Richmond for the biochemical facility, Dr. David Sargent for critical reading of the manuscript, and Dr. H. Gross, Dr. Roger A. Wepf, and Peter Tittmann in EMEZ (Electron microscopy center, Eidgenössische Technische Hochschule Zürich) for technical support.

This work was funded by a grant from the Swiss National Science Foundation and National Centres of Competence in Research Structural Biology (NF 3100A0-107540 to T. Ishikawa), Special Coordination Funds for Promoting Science and Technology (16083207 to K. Oiwa), and the Grant-in-Aid for Scientific Research on the Priority Area "Regulation of Nano-systems in Cells" by the Ministry of Education, Culture, Sports, Science and Technology (to K. Oiwa). All commercial affiliations/conflicts of interest have been disclosed.

Submitted: 11 August 2008
Accepted: 29 October 2008

References

Avolio, J., A.N. Glazzard, M.E. Holwill, and P. Satir. 1986. Structures attached to doublet microtubules of cilia: computer modeling of thin-section and negative-stain stereo images. *Proc. Natl. Acad. Sci. USA.* 83:4804–4808.

Bozkurt, H.H., and D.M. Woolley. 1993. Morphology of nexin links in relation to interdoublet sliding in the sperm flagellum. *Cell Motil. Cytoskeleton.* 24:109–118.

Burgess, S.A., D.A. Carter, S.D. Dover, and D.M. Woolley. 1991. The inner dynein arm complex: compatible images from freeze-etch and thin section methods of microscopy. *J. Cell Sci.* 100:319–328.

Burgess, S.A., M.L. Walker, H. Sakakibara, P.J. Knight, and K. Oiwa. 2003. Dynein structure and power stroke. *Nature.* 421:715–718.

Burgess, S.A., M.L. Walker, H. Sakakibara, H. Oiwa, and P.J. Knight. 2004. The structure of dynein-c by negative stain electron microscopy. *J. Struct. Biol.* 146:205–216.

Dymek, E.E., and E.F. Smith. 2007. A conserved CaM- and radial spoke associated complex mediates regulation of flagellar dynein activity. *J. Cell Biol.* 179:515–526.

Frank, J., M. Radermacher, P. Penczek, J. Zhu, Y.H. Li, M. Ladjadj, and A. Leith. 1996. SPIDER and WEB: processing and visualization of images in 3D electron microscopy and related fields. *J. Struct. Biol.* 116:190–199.

Gardner, L.C., E. O'Toole, C.A. Perrone, T. Giddings, and M.E. Porter. 1994. Components of a "dynein regulatory complex" are located at the junction between the radial spokes and the dynein arms in *Chlamydomonas* flagella. *J. Cell Biol.* 127:1311–1325.

Goodenough, U., and J. Heuser. 1984. Structural comparison of purified dynein proteins with in situ dynein arms. *J. Mol. Biol.* 180:1083–1118.

Goodenough, U.W., and J. Heuser. 1985. Substructure of inner dynein arms, radial spokes, and the central pair/projection complex of cilia and flagella. *J. Cell Biol.* 100:2008–2018.

Gorman, D.S., and R.P. Levine. 1965. Cytochrome f and plastocyanin: their sequence in the photosynthetic electron transport chain of *Chlamydomonas reinhardtii*. *Proc. Natl. Acad. Sci. USA.* 54:1665–1669.

Hendrickson, T.W., C.A. Perrone, P. Griffin, K. Wuichet, J. Mueller, P. Yang, M.E. Porter, and W.S. Sale. 2004. IC138 is a WD-repeat dynein intermediate chain required for light chain assembly and regulation of flagellar bending. *Mol. Biol. Cell.* 15:5431–5442.

Heymann, J.B. 2001. Bsoft: image and molecular processing in electron microscopy. *J. Struct. Biol.* 133:156–169.

Ishikawa, T., H. Sakakibara, and K. Oiwa. 2007. The architecture of outer dynein arms in situ. *J. Mol. Biol.* 368:1249–1258.

Johnson, K.A., and J.S. Wall. 1983. Structure and molecular weight of the dynein ATPase. *J. Cell Biol.* 96:669–678.

Kagami, O., and R. Kamiya. 1992. Translocation and rotation of microtubules caused by multiple species of *Chlamydomonas* inner-arm dynein. *J. Cell Sci.* 103:653–664.

Kamiya, R. 1988. Mutations at twelve independent loci result in absence of outer dynein arms in *Chlamydomonas reinhardtii*. *J. Cell Biol.* 107:2253–2258.

Kamiya, R. 2002. Functional diversity of axonemal dyneins as studied in *Chlamydomonas* mutants. *Int. Rev. Cytol.* 219:115–155.

Kamiya, R., E. Kurimoto, and E. Muto. 1991. Two types of *Chlamydomonas* flagellar mutants missing different components of inner-arm dynein. *J. Cell Biol.* 112:441–447.

Kato, T., O. Kagami, T. Yagi, and R. Kamiya. 1993. Isolation of two species of *Chlamydomonas reinhardtii* flagellar mutants, ida5 and ida6, that lack a newly identified heavy chain of the inner dynein arm. *Cell Struct. Funct.* 18:371–377.

Kikushima, K., and R. Kamiya. 2008. Clockwise translocation of microtubules by flagellar inner-arm dyneins in vitro. *Biophys. J.* 94:4014–4019.

King, S.M., and R. Kamiya. 2008. Axonemal dyneins: assembly, structure, and force generation. *In* Chlamydomonas Sourcebook, Vol. 3. Cell Motility and Behavior. G. Witman, editor. Elsevier Press, Amsterdam. In press.

Kotani, N., H. Sakakibara, S.A. Burgess, H. Kojima, and K. Oiwa. 2007. Mechanical properties of inner-arm dynein-f (dynein I1) studied with in vitro motility assays. *Biophys. J.* 93:886–894.

Kremer, J.R., D.N. Mastronarde, and J.R. McIntosh. 1996. Computer visualization of three-dimensional image data using IMOD. *J. Struct. Biol.* 116:71–76.

LeDizet, M., and G. Piperno. 1995. The light chain p28 associates with a subset of inner dynein arm heavy chains in *Chlamydomonas* axonemes. *Mol. Biol. Cell.* 6:697–711.

Lupetti, P., S. Lanzavecchia, D. Mercati, F. Cantele, R. Dallai, and C. Mencarelli. 2005. Three-dimensional reconstruction of axonemal outer dynein arms in situ by electron tomography. *Cell Motil. Cytoskeleton.* 62:69–83.

Mastronarde, D.N. 1997. Dual-axis tomography: an approach with alignment methods that preserve resolution. *J. Struct. Biol.* 120:343–352.

Mastronarde, D.N., E.T. O'Toole, K.L. McDonald, J.R. McIntosh, and M.E. Porter. 1992. Arrangement of inner dynein arms in wild-type and mutant flagella of *Chlamydomonas*. *J. Cell Biol.* 118:1145–1162.

Nicastro, D., J.R. McIntosh, and W. Baumeister. 2005. 3D structure of eukaryotic flagella in a quiescent state revealed by cryo-electron tomography. *Proc. Natl. Acad. Sci. USA.* 102:15889–15894.

Nicastro, D., C. Schwartz, J. Pierson, R. Gaudette, M.E. Porter, and J.R. McIntosh. 2006. The molecular architecture of axonemes revealed by cryoelectron tomography. *Science.* 313:944–948.

Nickell, S., F. Förster, A. Linaroudis, W.D. Net, F. Beck, R. Hegerl, W. Baumeister, and J.M. Plitzko. 2005. TOM software toolbox: acquisition and analysis for electron tomography. *J. Struct. Biol.* 149:227–234.

Oda, T., N. Hirokawa, and M. Kikkawa. 2007. Three-dimensional structures of the flagellar dynein-microtubule complex by cryoelectron microscopy. *J. Cell Biol.* 177:243–252.

Perrone, C.A., S.H. Myster, R. Bower, E.T. O'Toole, and M.E. Porter. 2000. Insights into the structural organization of the I1 inner arm dynein from a domain analysis of the 1beta dynein heavy chain. *Mol. Biol. Cell.* 11:2297–2313.

Pettersen, E.F., T.D. Goddard, C.C. Huang, G.S. Couch, D.M. Greenblatt, E.C. Meng, and T.E. Ferrin. 2004. UCSF chimera - a visualization system for exploratory research and analysis. *J. Comput. Chem.* 25:1605–1612.

Piperno, G., Z. Ramanis, E.F. Smith, and W.S. Sale. 1990. Three distinct inner dynein arms in *Chlamydomonas* flagella: molecular composition and location in the axoneme. *J. Cell Biol.* 110:379–389.

Piperno, G., K. Mead, and W. Shestak. 1992. The inner dynein arms I2 interact with a "dynein regulatory complex" in *Chlamydomonas* flagella. *J. Cell Biol.* 118:1455–1463.

Piperno, G., K. Mead, M. LeDizet, and A. Moscatelli. 1994. Mutations in the "dynein regulatory complex" alter the ATP-insensitive binding sites for inner arm dyneins in *Chlamydomonas* axonemes. *J. Cell Biol.* 125:1109–1117.

Porter, M.E. 1996. Axonemal dyneins: assembly, organization, and regulation. *Curr. Opin. Cell Biol.* 8:10–17.

Porter, M.E., J. Power, and S.K. Dutcher. 1992. Extragenic suppressors of paralyzed flagellar mutations in *Chlamydomonas reinhardtii* identify loci that alter the inner dynein arms. *J. Cell Biol.* 118:1163–1176.

Rupp, G., and M.E. Porter. 2003. A subunit of the dynein regulatory complex in *Chlamydomonas* is a homologue of a growth arrest–specific gene product. *J. Cell Biol.* 162:47–57.

Samso, M., and M.P. Koonce. 2004. 25 angstrom resolution structure of a cytoplasmic dynein motor reveals a seven-member palnar ring. *J. Mol. Biol.* 340:1059–1072.

Taylor, H.C., P. Satir, and M.E. Holwill. 1999. Assessment of inner dynein arm structure and possible function in ciliary and flagellar axonemes. *Cell Motil. Cytoskeleton.* 43:167–177.

Wirschell, M., T. Hendrickson, and W.S. Sale. 2007. Keeping and eye on I1: I1 dynein as a model for flagella dynein assembly and regulation. *Cell Motil. Cytoskeleton.* 64:569–579.

Witman, G.B. 1986. Isolation of *Chlamydomonas* flagella and flagellar axonemes. *Methods Enzymol.* 134:280–290.

Yagi, T., I. Minoura, A. Fujiwara, R. Saito, T. Yasunaga, M. Hirono, and R. Kamiya. 2005. An axonemal dynein particularly important for flagellar movement at high viscosity. Implications from a new *Chlamydomonas* mutant deficient in the dynein heavy chain gene DHC9. *J. Biol. Chem.* 280:41412–41420.

Yanagisawa, H.A., and R. Kamiya. 2001. Association between actin and light chains in *Chlamydomonas* flagellar inner-arm dyneins. *Biochem. Biophys. Res. Commun.* 288:443–447.